Defect Prediction in Directed Energy Deposition Using an Ensemble of Clustering Models

Shawqi Mohammed Farea, Mustafa Unel, Bahattin Koc
Faculty of Engineering and Natural Sciences
Integrated Manufacturing Technologies Research and Application Center
Sabanci University
Istanbul, Turkey
munel@sabanciuniv.edu

***Abstract*—Directed energy deposition (DED) stands as a pivotal additive manufacturing technique, revolutionizing the landscape of modern manufacturing. However, process-related defects hinder its broad application across different sectors. In this paper, we propose a novel methodology for the in-situ prediction of defects in DED processes based on the thermal images of the melt pools. Initially, multiple features, summarizing the thermal and geometric characteristics of the melt pool, were extracted. Based on these features, an ensemble of unsupervised clustering models was constructed to distinguish anomalies – images with defects – from the defect-free images. Roughly 3% of the acquired images were predicted to include defects. Upon visual inspection, these images exhibited distinctive thermal distributions and geometric configurations compared to the remaining dataset. Furthermore, a 2D approximate visualization of the feature space revealed the clustering structure of the thermal images in their feature space. This visualization showed that the anomalies could be distinguished from the majority of normal images, which further validates the prediction model's effectiveness.**

***Index Terms*—additive manufacturing, DBSCAN clustering, defect detection, directed energy deposition, IN718 superalloy**

I. Introduction

Directed energy deposition (DED) is one of the promising additive manufacturing processes that can additively manufacture dense metal parts with functional geometries and enhanced mechanical properties. This digital manufacturing technology is particularly suitable for prototyping, repairing, and modifying metal parts [1]. It is also known for its short manufacturing times and high material utilization. Due to these unparalleled characteristics, DED finds widespread application across diverse industries, including aerospace, automotive, medical, and beyond.

Based on computer-aided design (CAD) files, DED processes utilize a high-energy heat source to melt the deposition feedstock and print the ultimate part incrementally, track-by-track and layer-by-layer. The heat source typically affixed to a multi-axis computer numerical control (CNC) head can be a laser, a plasma arc, or an electron beam. Conversely, the feedstock delivered via a nozzle is available in either powder or wire forms. The feedstock material can be metals, ceramics, or even a composite of both; however, DED is widely used for printing metals and is alternatively known as directed metal deposition accordingly.

This work was funded by TUBITAK with grant number 20AG050

The main limitation of DED processes, which impedes its widespread adoption across different sectors, stems from in-situ evolving defects such as lack of fusion, cracking, porosity, and surface roughness. Such defects lead to poor mechanical properties and reduced quality of final parts [2]. The prime root causes of these defects are due to feedstock quality (like impurity or feedstock porosity), non-optimized process variables (e.g., the laser power and scan spacing/speed), the high thermal gradients, and rapid cooling rates [3].

Comprehension of the intricate physics underlying DED processes remains a significant challenge due to their intrinsic complexity. This hampers the construction of a prior physics-based model summarizing the correlation between the process variables and the potential formulation of defects. As a traditional approach, these defects are identified through post-process inspection methods, such as metallurgical analysis or computed tomography (CT); nonetheless, these methods are expensive and time-consuming.

Alternatively, the detection and subsequent elimination (or at least reduction) of the developed defects can be conducted through real-time monitoring of the melt pool, combined with feedback control and process optimization [3]. To this end, thermal cameras and temperature sensors have been commonly employed in the literature to capture the thermal distribution and geometry of the melt pool. The formulation of microstructural defects is expected to be manifested in the melt pool's thermal dynamics captured by its thermal image. Therefore, this close relation between the melt pool characteristics and defect formulation can be modeled using machine learning (ML) techniques.

Khanzadeh et al. [4] implemented multiple classical ML methods; namely linear discriminant analysis, quadratic discriminant analysis, k-nearest neighbors (KNN), decision trees, and support vector machine (SVM); for in-situ porosity prediction. On the other hand, Gaja et al. [5] used classifiers based on artificial neural networks (ANN) and logistic regression to detect developed defects such as cracks and porosity. In addition, various convolutional neural network (CNN) architectures; e.g., AlexNet, VGG16, ResNet, and GoogleNet; have

been proposed to detect defects including rough texture, lack of fusion, porosity, and cracks [6]–[9]. Tian et al. [10], on the other hand, proposed the combination of CNN and recurrent neural network (RNN) classifiers for porosity detection by fusing thermal images acquired by the built-in pyrometer and thermal camera.

Nevertheless, the existing studies in this research line have tackled this problem as a supervised classification problem. This formulation has many drawbacks. For instance, it suffers from an imbalanced data issue that significantly affects the classifier performance. Additionally, in this formulation, defect detection is not generic with respect to all defect classes since the defect class used for training represents only a single class (or a few classes in the case of multiclass classification). An alternative yet effective approach is to formulate defect detection as an unsupervised (or at least semi-supervised) problem in accordance with its inherent nature as a subcategory of anomaly detection. As one of a few works in this direction, K-means [11] and self-organizing maps (SOM) [12], [13] have been utilized to detect porosities and cracks.

In this paper, we propose an ensemble of unsupervised clustering models to predict defects in laser directed energy deposition (L-DED). The main contributions of this work, in addition to data collection and preparation, are as follows:

1) Extraction of relevant features summarizing the thermal dynamics and geometric properties of the melt pools.
2) A generic framework, irrespective of defect class, for predicting defects developed in DED samples, approaching the defect detection problem from an anomaly detection perspective. This framework can also serve as an automatic tool for (weakly) labeling data without the need for post-process inspection techniques, such as micro CT.
3) Validation of the results by investigating a 2D approximate visualization of the feature space.

The rest of this paper is organized as follows: The proposed methodology for defect detection is detailed in Section II, and the obtained results are presented and discussed in Section III. Finally, Section IV offers the concluding remarks for the paper.

II. Defect Detection Methodology

In this section, the proposed methodology for defect detection in DED-manufactured parts is explained in detail. An overview of the methodology is shown in Fig. 1. This approach comprises five main steps, namely threshold segmentation, feature extraction, normalization, clustering, and visualization. These steps are illustrated further in the subsequent subsections.

A. Threshold Segmentation

As the first step, the melt pool was extracted from each input thermal image. The threshold temperature of the melt pool is specified as 1560 °C. Accordingly, the biggest region in the image whose temperature is at least the same as the threshold temperature was extracted. This region corresponds to the melt pool in that image. Fig. 2 shows a sample image with its segmented binary and thermal images. The binary image is used for extracting the shape features, as explained in detail later. In contrast, histogram-based color and texture features are extracted from the segmented thermal image.

B. Feature Extraction

From each image, three sets of features were extracted. These sets are shape features, histogram-based color features, and texture features, as listed in Table I and illustrated further in the following subsections.

1) Shape features: As shape features, the area, major axis length, eccentricity, and circularity were extracted from the binary image that was segmented from the input thermal image as explained in the previous subsection. These features summarize the melt pool geometry, and they help in detecting defects like lack of fusion, underheating, and distorted shapes of melt pools.

2) Color features: Color features, on the other hand, were extracted from the segmented thermal image of the melt pool. These features rely on the histogram of that extracted region (i.e., the temperature distribution of the melt pool), and they may detect defects that shape features alone fail to detect, e.g., overheating. These features include the mean, standard deviation, skewness, and entropy of the extracted melt poot temperatures.

3) Texture features: Texture features are extracted based on the gray-level co-occurrence matrix (GLCM). The GLCM summarizes the spatial relationship between pairs of pixels. It is formed by computing how often pairs of pixels with particular values and predefined spatial relationships occur in the image. These spatial relationships between pairs of pixels are determined by two user-chosen parameters, the distance and angle of the relationship. After the GLCM has been formed, four statistical measures – namely, energy, correlation, contrast, and homogeneity – will be extracted from the GLCM matrix.

C. Normalization

The extracted features have inconsistent scales, leading to the dominance of the high-scale features. To address this concern, these features were normalized by initially subtracting their means and subsequently dividing by their standard deviations. This normalization scheme (see [14]) results in the different features having consistent scales. As a result, the contributions of the features during the training process become equalized. This most frequently leads to a significant

TABLE I
List of Extracted Features

Shape features	Color features	Texture features
Area	Mean	Energy
Major axis length	Standard deviation	Correlation
Eccentricity	Skewness	Contrast
Circularity	Entropy	Homogeneity

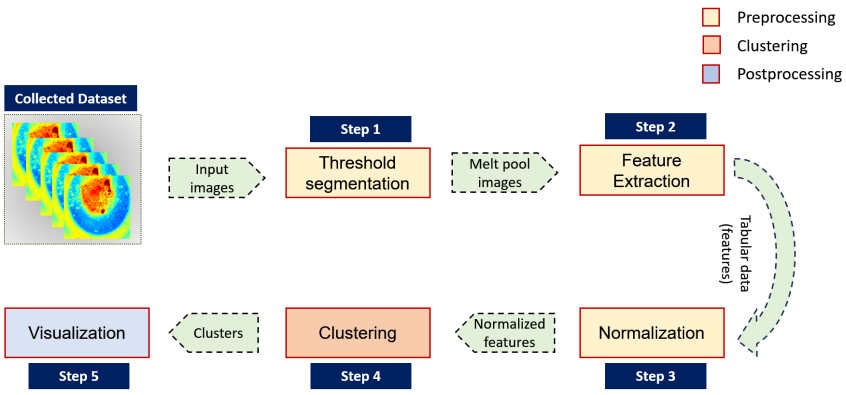

Fig. 1. The block diagram of the proposed methodology.

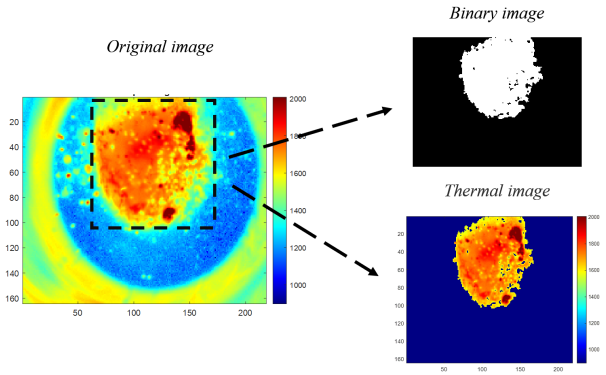

Fig. 2. Segmentation of a sample image into its corresponding segmented binary and thermal images.

improvement in the numerical stability and accuracy of the ML algorithm.

D. Clustering

The main purpose of the defect detection framework is to distinguish anomaly images (i.e., images with defects) from normal (i.e., defect-free) images based on their normalized extracted features. To that end, an unsupervised clustering approach was proposed in this study, given the advantages associated with the unsupervised formulation of the problem, as detailed in Section I. The proposed clustering approach is an ensemble of DBSCAN (density-based spatial clustering of applications with noise) models. DBSCAN is an unsupervised clustering algorithm with a high ability to identify outliers (or anomalies). Compared to other ML clustering algorithms such as K-means and SOM, DBSCAN does not require specifying the number of clusters beforehand. It separates the data into one or more normal clusters besides outliers, i.e., data instances not belonging to any cluster. The algorithm has the following two parameters (for more details about this algorithm and its parameters, the reader is recommended to refer to [15]):

1) **Eps (ϵ):** indicates the maximum distance between neighbor points (Eps is also known as the neighborhood search radius and it is the key parameter).
2) **MinPts:** indicates the minimum number of neighbor points for a core point (it determines the minimum size of any cluster)

According to these parameters, the data points can be categorized into:

1) **Core point:** a point which has at least MinPts points in its ϵ-neighborhood (core points lie inside clusters).
2) **Border point:** a point which is in the ϵ-neighborhood of a core point (border points lie at the boundaries of the clusters).
3) **Noise point:** a point which is neither a core point nor a border point (noise points are also known as outlier points or anomalies).

Different values of these two parameters lead to different DBSCAN models. In this work, four different values of Eps ($\{1, 1.5, 2, 2.5\}$) and four different values of MinPts ($\{11, 16, 21, 26\}$) were selected in light of the guidelines proposed in [15] while maintaining sufficient distance among themselves to increase the independence of their corresponding models. Therefore, an ensemble of 16 DBSCAN models was constructed based on a voting scheme. That is, a data point (an image) will be considered as an outlier only if it is labeled as such by at least nine models. This approach helps to deal with the unlabeled data with unknown ground-truth labels. The basic intuition is that if most models give a data point the same label, then the ground-truth label for that data point is most likely to be the same as the predicted label. That is because it is less probable for most models to simultaneously mislabel a data point, especially if these models are independent.

E. Visualization

As a postprocessing step, the extracted features were visualized in a 2D space while highlighting the anomalies detected by the DBSCAN ensemble; the main goal is to search for spatial separability between these anomalies and the normal data. Additionally, we aim to investigate the clustering nature

of all data in this 2D embedding, which serves as a good approximation of the original feature space. To do so, we implement t-SNE (t-distributed Stochastic Neighbor Embedding) [16], a nonlinear dimensionality reduction algorithm. While projecting the data into a 2D space, t-SNE attempts to preserve the spatial arrangement of the data in their original feature space. In other words, the clustering nature of the projected data in the 2D space is assumed to reflect the real clustering nature of the data in its original feature space. Therefore, this postprocessing step can be also used to validate the results of the DBSCAN ensemble.

III. Experimental Results

The collected dataset consists of thermal images of melt pools acquired by a LASERTEC 65 DED hybrid machine. As shown in Fig. 3, this DMG MORI-manufactured machine is equipped with a co-axial nozzle, laser/optic system, and powder delivery. The thermal camera monitors the DED process by capturing the temperature distribution of the melt pool whereas the co-axial nozzle facilitates the flow of the powder feedstock carried by argon gas. In this paper, the feedstock material is Inconel 718 (IN718), a corrosion-resistant, high-strength nickel-chromium superalloy. IN718 has been widely used in critical applications, such as nuclear reactors and aerospace engines, due to its favorable mechanical properties, high-temperature oxidation resistance, and good weldability [17], [18].

The total collected dataset comprises 2295 thermal images, each of which has a standard resolution of 164 x 218. A sample thermal image of the melt pool is provided in Fig. 4, alongside its 3D temperature distribution and histogram. The temperature histogram appears to be multimodal. Its first mode is at around 1200 °C, which represents the background, the second mode is at nearly 1550 °C, representing the heat-affected nozzle tip and boundary of the melt pool, while the last mode is at almost 1750 °C, which is the core of the melt pool.

Lastly, it is worth mentioning that the collected data are unlabeled, without any prior knowledge of the ground-truth labels. Like any other additive manufacturing processes, the accurate labeling of the data collected from DED processes is highly expensive and cumbersome.

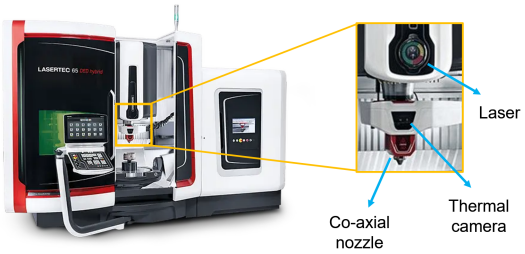

Fig. 3. LASERTEC 65 DED hybrid machine [19].

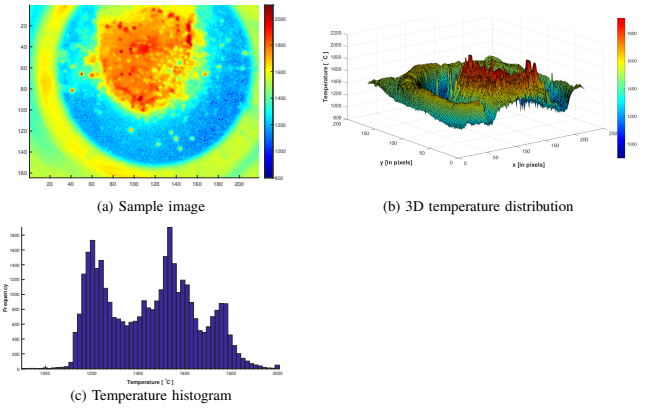

(a) Sample image

(b) 3D temperature distribution

(c) Temperature histogram

Fig. 4. A sample thermal image with its temperature distribution and histogram.

A. DBSCAN clustering

As stated in the previous section, an ensemble of 16 DBSCAN models was implemented as the clustering algorithm. These 16 models were constructed by choosing four different values of both MinPts and Eps whilst the distance measure was set as Euclidian distance. As presented in Table II, the DBSCAN ensemble detected two structured clusters besides some anomalies (i.e., outliers) in the feature space. Most of the images (2228 images) were assigned to Cluster 1 while only 25 images were assigned to Cluster 2. The remaining 42 images, not having been assigned to either cluster, were labeled as anomalies. As most of the images were assigned to Cluster 1, it represents the normal cluster (i.e., the cluster of defect-free images). On the other hand, Cluster 2 may correspond to group anomalies (images with defects) instead of normal images owing to the small size of this cluster. Therefore, it will be investigated more below.

To visually inspect the achieved results, four sample images from each cluster as well as four sample images from the detected anomalies were randomly selected and displayed in Fig. 5. Below each image, the number of models labeling that image as such is given for each cluster. By scrutinizing the images, detected anomalies are clearly distinctive from the sample normal images (Cluster 1 images). These anomalies suffer from either overheating (see the second image in the anomalies row in Fig. 5) or underheating with distorted shapes of their melt pools (see the remaining images in the same row). While underheating leads to a lack of fusion which in turn contributes to the porosity formulation, overheating is another issue resulting in increased surface roughness and inferior mechanical [20]. The sample images from Cluster 2 have melt pools with slightly distorted shapes or a moderate overheating issue. Interestingly, these samples were labeled

TABLE II
Results of DBSCAN Ensemble

Cluster	Cluster 1	Cluster 2	Anomalies
# images	2228	25	42

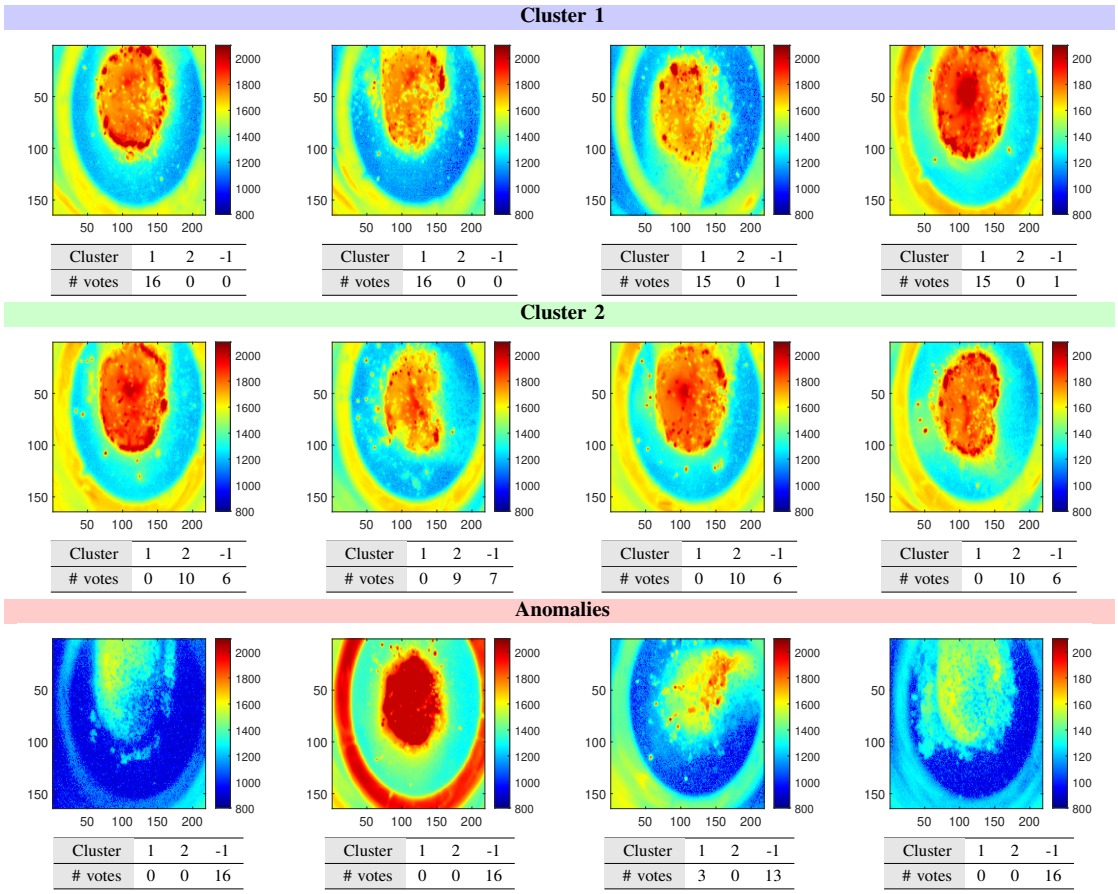

Fig. 5. Sample images from both clusters and detected anomalies (the number of votes for each cluster is shown below each image where -1 corresponds to anomalies).

as anomalies by at least six models. Therefore, Cluster 2 is expected to represent group anomalies (i.e., anomalies constructing a cluster among themselves) as opposed to the point anomalies, that are not belonging to any cluster.

B. 2D visualization

As a postprocessing step, the clustering structure of thermal images is investigated. As shown in Fig. 6, the images, represented by their extracted features in the feature space, were projected into a 2D space using the dimensionality reduction algorithm, t-SNE. The structure of the projected data approximates the original structure in the feature space. According to Fig. 6, Cluster 1 and Cluster 2 are mostly separatable from one another while anomalies lie at the boundaries of both clusters. In addition to the visual inspection of the sample images in Fig. 5, this also validates the obtained results where the detected point and group anomalies (Cluster 2) are located far away from the vast majority of normal data (Cluster 1).

IV. Conclusion

Despite its favorable advantages, directed energy deposition (DED) still suffers from the in-process evolution of defects, a key limitation impeding its widespread application. Undetected defects result in final parts with inferior mechanical properties and reduced quality. This work proposed an unsupervised framework for defect detection, regardless of defect class. This framework is based on an ensemble of DBSCAN models applied to relevant features extracted from thermal images of the melt pools. The unsupervised formulation of the problem enabled a generic approach and simultaneously

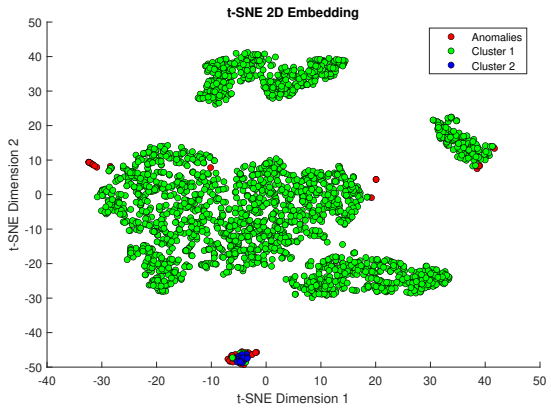

Fig. 6. t-SNE visualization of the ten selected features (the detected clusters and anomalies are shown).

mitigated the notorious imbalanced data issue, an inherent characteristic of defect detection. The obtained results were validated by the visual inspection of some sample images and investigation of a 2D approximate visualization of the feature space. According to both, the detected anomalies appear distinctive from the vast majority of normal images.

The proposed methodology can be utilized for (weakly) labeling defect detection datasets in an automatic manner without the need for post-process inspection techniques, known for their high cost and time consumption. Another future research direction is the development of an end-to-end defect detection approach, in which the DBSCAN ensemble is applied to features extracted by a deep learning technique, e.g., deep autoencoders.

ACKNOWLEDGMENT

The support provided by TUBITAK through the grant 20AG050 is gratefully acknowledged.

REFERENCES

[1] S. J. Wolff, H. Wu, N. Parab, C. Zhao, K. F. Ehmann, T. Sun, and J. Cao, "In-situ high-speed x-ray imaging of piezo-driven directed energy deposition additive manufacturing," *Scientific reports*, vol. 9, no. 1, p. 962, 2019.

[2] K. Zhu, J. Y. H. Fuh, and X. Lin, "Metal-based additive manufacturing condition monitoring: A review on machine learning based approaches," *IEEE/ASME Transactions on Mechatronics*, vol. 27, no. 5, pp. 2495–2510, 2021.

[3] D. Svetlizky, M. Das, B. Zheng, A. L. Vyatskikh, S. Bose, A. Bandyopadhyay, J. M. Schoenung, E. J. Lavernia, and N. Eliaz, "Directed energy deposition (ded) additive manufacturing: Physical characteristics, defects, challenges and applications," *Materials Today*, vol. 49, pp. 271–295, 2021.

[4] M. Khanzadeh, S. Chowdhury, M. Marufuzzaman, M. A. Tschopp, and L. Bian, "Porosity prediction: Supervised-learning of thermal history for direct laser deposition," *Journal of Manufacturing Systems*, vol. 47, pp. 69–82, 2018.

[5] H. Gaja and F. Liou, "Defect classification of laser metal deposition using logistic regression and artificial neural networks for pattern recognition," *The International Journal of Advanced Manufacturing Technology*, vol. 94, pp. 315–326, 2018.

[6] B. Zhang, S. Liu, and Y. C. Shin, "In-process monitoring of porosity during laser additive manufacturing process," *Additive Manufacturing*, vol. 28, pp. 497–505, 2019.

[7] W. Cui, Y. Zhang, X. Zhang, L. Li, and F. Liou, "Metal additive manufacturing parts inspection using convolutional neural network," *Applied Sciences*, vol. 10, no. 2, p. 545, 2020.

[8] Q. Tian, S. Guo, Y. Guo *et al.*, "A physics-driven deep learning model for process-porosity causal relationship and porosity prediction with interpretability in laser metal deposition," *CIRP Annals*, vol. 69, no. 1, pp. 205–208, 2020.

[9] D. B. Patil, A. Nigam, S. Mohapatra, and S. Nikam, "A deep learning approach to classify and detect defects in the components manufactured by laser directed energy deposition process," *Machines*, vol. 11, no. 9, 2023.

[10] Q. Tian, S. Guo, E. Melder, L. Bian, and W. G. Guo, "Deep learning-based data fusion method for in situ porosity detection in laser-based additive manufacturing," *Journal of Manufacturing Science and Engineering*, vol. 143, no. 4, p. 041011, 2021.

[11] H. Gaja and F. Liou, "Defects monitoring of laser metal deposition using acoustic emission sensor," *The International Journal of Advanced Manufacturing Technology*, vol. 90, pp. 561–574, 2017.

[12] A.-I. García-Moreno, "Automatic quantification of porosity using an intelligent classifier," *The International Journal of Advanced Manufacturing Technology*, vol. 105, pp. 1883–1899, 2019.

[13] M. Khanzadeh, S. Chowdhury, M. A. Tschopp, H. R. Doude, M. Marufuzzaman, and L. Bian, "In-situ monitoring of melt pool images for porosity prediction in directed energy deposition processes," *IISE Transactions*, vol. 51, no. 5, pp. 437–455, 2019.

[14] K. Cabello-Solorzano, I. Ortigosa de Araujo, M. Peña, L. Correia, and A. J. Tallón-Ballesteros, "The impact of data normalization on the accuracy of machine learning algorithms: A comparative analysis," in *International Conference on Soft Computing Models in Industrial and Environmental Applications*. Springer, 2023, pp. 344–353.

[15] M. Ester, H.-P. Kriegel, J. Sander, X. Xu *et al.*, "A density-based algorithm for discovering clusters in large spatial databases with noise," in *kdd*, vol. 96, no. 34, 1996, pp. 226–231.

[16] L. Van der Maaten and G. Hinton, "Visualizing data using t-sne." *Journal of machine learning research*, vol. 9, no. 11, 2008.

[17] M. Ma, Z. Wang, and X. Zeng, "Effect of energy input on microstructural evolution of direct laser fabricated in718 alloy," *Materials Characterization*, vol. 106, pp. 420–427, 2015.

[18] S. Zhang, X. Lin, L. Wang, X. Yu, Y. Hu, H. Yang, L. Lei, and W. Huang, "Strengthening mechanisms in selective laser-melted inconel718 superalloy," *Materials Science and Engineering: A*, vol. 812, p. 141145, 2021.

[19] DMG MORI. (Accessed: 2024). [Online]. Available: https://en.dmgmori.com/

[20] R. Ranjan, Z. Chen, C. Ayas, M. Langelaar, and F. Van Keulen, "Overheating control in additive manufacturing using a 3d topology optimization method and experimental validation," *Additive Manufacturing*, vol. 61, p. 103339, 2023.